Behaviour of aircraft composite panels under impact: Influence of impactor, loading and strain rate

Helder Martins
helder.martins@tecnico.ulisboa.pt

Instituto Superior Técnico, Universidade de Lisboa, Portugal

December 2020

Abstract: Composite materials are being increasingly used in aerospace structures because of their excellent mechanical characteristics, such as stiffness and strength. However, this material has comparatively weak mechanical properties, such as brittleness and delamination in the through-thickness direction, which makes it more susceptible to localized loadings, such as impacts. During the useful life, and even in maintenance, an aircraft can be subjected to several types of collisions. Hence, it is very important to study impacts on these structures. This work presents a numerical study on the mechanical behaviour of composite (carbon-fibre reinforced polymer) fuselage panels subjected to impact through dynamic finite element analyses performed in Abaqus/Explicit. Initially, a brief introduction to the topic and a literature review is presented. Then, the numerical models are described in detail. Afterwards, the numerical results for the reference panel (with T-shaped stringers) impacted by two different materials (steel and ice) are presented. In both cases, two levels of preloads were used (15 and 30% of the buckling load) applied either in compression or in tension. Also, regarding ice projectiles, the influence of pressurization is investigated. For ice, only spherical geometries are used whereas for steel three geometries are tested: spherical, cylindrical and conical. Then, the influence of the stringer geometry (I, C, J and Ω) on the strength of the panel is investigated, by replicating the preloads that induce higher residual velocities in the panel with T-shaped stringers. The strain rate effect on the mechanical properties is considered in the simulations and an elastic behaviour is assumed for both projectiles (steel and ice). Finally, the main conclusions and possible future developments are presented.

Keywords: Impact loading, CFRP panels, residual velocity, strain rate, preloads

1. Introduction

Carbon Fibre Reinforced Polymer (CFRP) composites are increasingly being used in the aerospace sector due to their high specific stiffness and strength, lightweight and corrosion and fatigue resistance [1]. However, despite their advantages, composite structures are more susceptible to transverse impact loading when compared to metallic materials. Since various objects may impact aerospace structures, during their lifetime, and in maintenance actions, an important design requirement for composite structures is their ability to tolerate impact damage [2].

This work intends to evaluate the influence of preloads (in tension and in compression) and of pressurization on the mechanical behaviour of reinforced composite panels subjected to transverse impact loading. Firstly, a parametric study is conducted on a panel with T-shaped stringers, considering the strain rate effects on the composite material and an elastic constitutive relation for the projectile. Afterwards, the type of stringer (I, C, J or Ω) that maximizes the resistance and decreases the brittleness of the panel is assessed for the most demanding conditions previously determined for the panel with the T-shaped stringers.

2. Literature review

During flight operations, due to the lift on the wings and horizontal stabilizer, the fuselage undergoes bending, which causes compressive axial loads [1] that can lead to buckling, post-buckling or even the collapse of the structure [3]. During cruise, the pressure difference between the interior and exterior of the fuselage varies between 40 and 50

kPa [4]. This pressure difference results in hoop stresses on the skin. For cylindrical fuselages, the hoop stresses are obtained through the following expression,

$$\sigma_H = \frac{P_i R}{t} \quad (1)$$

where P_i represents the internal pressure, R the radius of the fuselage and t the thickness of the skin.

Besides the stresses previously mentioned, the aircraft can also find during its operation, and even in maintenance, various types of impact loading, which can compromise the integrity of the structure. For this reason, the behaviour of aerospace structures under different impact loadings has been researched in several works (both experimental and numerical). To frame some studies, carried out over the last decade, the concepts of residual velocity and ballistic limit need to be firstly defined. The former is defined as the velocity of the projectile after completely penetrating a given target [5]. Regarding the ballistic limit, there are currently two definitions in the available literature: on the one hand, Pernas-Sánchez *et al.* [6] define it as the minimum velocity required to fully penetrate a target and, on the other hand, Silva *et al.* [7] consider that it is the initial velocity that the projectile must have so that there is a 50% probability of fully penetrating a target.

Regarding the influence of the impactor, Pernas-Sánchez *et al.* [8] developed a numerical model (using the commercial finite element software LS-DYNA v.R7) to study the influence of the dimension of spherical projectiles in high-speed impacts on carbon/epoxy plates. These authors concluded that the residual velocity increases with the increase in the sphere's radius. Fonseca *et al.* [9] studied the impact response in fuselage panels with T-, I-, C-, J- and Ω-shaped stringers. Using the commercial finite element software Abaqus, these authors concluded that the stringer geometry that maximizes the resistance (lowers residual velocity) is the I-shaped. These authors also performed a parametric study in the most resistant panel to study the influence of the projectile's size and geometry. They concluded that the smaller the projectile's dimensions the higher the residual velocity. Additionally, Fonseca *et al.* [9] found that the flatter the projectile's impact surface the lower the residual velocity tends to be.

Besides the influence of the projectile's dimensions, an essential prerequisite for successfully modelling the impact response of a structure is the understanding of the mechanical properties of the materials used in the structure. For composite materials, the properties of highest interest are the modulus of elasticity and maximum strengths. These usually depend on the strain rate, $\dot{\varepsilon}$, that is defined according to the following equation [10],

$$\dot{\varepsilon} = \frac{d\varepsilon}{dt} \quad (2)$$

where $\frac{d\varepsilon}{dt}$ is the variation of strain with time.

The range of strain rates encountered in the impact of composite structures may be very wide, from as low as 1 s^{-1} or less, in low-velocity soft-body impacts on large structures, to well over 1000 s^{-1}, in regions of localized deformation associated with high-velocity impacts. Thus, several studies have been conducted, up to date, to determine the effect of strain rate on the mechanical responses of composite materials. Schaefer *et al.* [11] proposed that the modulus of elasticity in the transverse direction (E_2) and the shear modulus (G_{12}) vary linearly with the logarithm of strain rate,

$$E(\dot{\varepsilon}) = E(\dot{\varepsilon}_0)\left(m_e \log_{10}\frac{\dot{\varepsilon}}{\dot{\varepsilon}_0} + 1\right) \quad (3)$$

where E may represent E_2 or G_{12}, m_e = 0.035 and $\dot{\varepsilon}_0$ is a reference strain rate (10^{-4} s^{-1}).

The authors also proposed a linear variation with the logarithm of strain rate for the transverse compressive (S_{c2}), transverse tensile (S_{t2}), and shear strengths (S_{s12}) according to,

$$F(\dot{\varepsilon}) = F(\dot{\varepsilon}_0)\left(m_f \log_{10}\frac{\dot{\varepsilon}}{\dot{\varepsilon}_0} + 1\right) \quad (4)$$

where F may represent S_{c2}, S_{t2}, or S_{s12}, m_f = 0.055 and $\dot{\varepsilon}_0$ is a reference strain rate (10^{-4} s^{-1}).

3. Numerical models

3.1. Geometry and mesh

Figure 1 shows the geometry and mesh of the reference panel (with T-shaped stringers) subjected to transverse impact loading by a spherical projectile. The panel has a total length

L = 780 mm, a radius R = 1000 mm and an arc length a = 560 mm. The five equally spaced stringers have flange heights h = 14 mm and blade widths b = 32 mm. The skin and stringers are bounded by a thin layer of adhesive (with 0.2 mm of thickness). The stacking sequences used in the panel were $[90, +45, -45, 0]_s$, $[(45, -45)_3, 0_6]$ (from top to bottom) and $[(45, -45)_3, 0_6]_s$ for the skin, flanges and blades respectively. Each layer has a thickness of 0.125 mm, which means that the total thicknesses of the skin, flanges and blades are 1.0, 1.5, and 3.0 mm, respectively. The diameter of the spherical projectile is D = 33 mm.

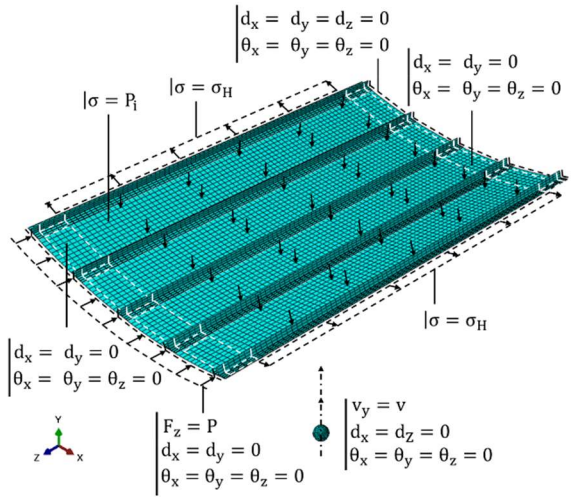

Figure 1: Geometry and mesh of (reference) panel with five T-shaped stringers.

The skin and stringers were modelled by 4 nodes shell elements (S4 in Abaqus [12] nomenclature) and the adhesive layer by 8 nodes solid cohesive elements (COH3D8 in Abaqus [12] nomenclature). The projectile was discretized by 8 nodes solid elements (C3D8 in Abaqus [12] nomenclature). In the skin, 78 finite elements (FE) were used along the longitudinal direction (z-axis) and along the width (x-axis): 10 FE between stringers and the same number of FE as those of the stringer's flange applied along the width (x-axis) in the stringer position. Regarding the adhesive, also 78 FE were used along the longitudinal direction (z-axis), 1 FE in the height direction (y-axis) and in the width direction (x-axis) the same number of FE used on the width (x-axis) of the flange. Regarding the stringers, 6 FE were used along the width (x-axis), 3 along the height (y-axis) of the blades and 78 FE along the longitudinal direction (z-axis). The projectile was discretized with 1536 FE.

Four additional cross-section shapes of stringers were studied: I-, C- J- and Ω-shaped stringers. The criterion for the design of the additional cross-sections was that the cross-section area was maintained (and equal to that of the T-shaped stringer) and the blade height had always 14 mm. Figure 2 shows the different cross-sections of stringers studied.

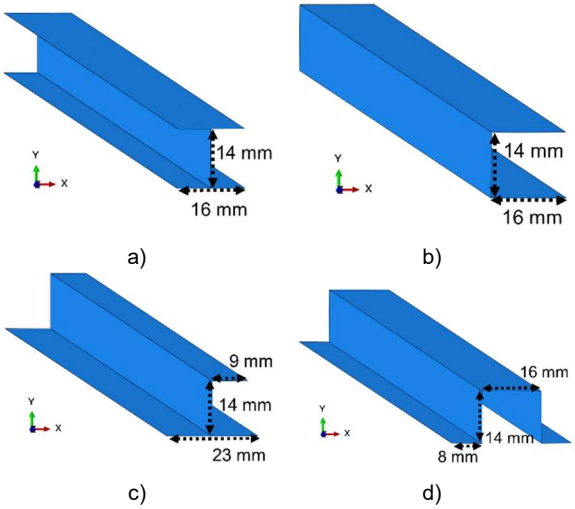

Figure 2: Geometry of alternative stringers: a) I, b) C, c) J and d) Ω.

The additional panels were modelled with the same number of FE as those of the reference panel along the longitudinal direction (z-axis), skin width (between stringers) and heights (y-axis) of the adhesive and blades. However, since all the additional configurations have an extra flange, compared to the reference configuration, adaptations were made on the stringer position. Configurations I and C were modelled using 4 FE along the width (x-axis) of the lower and upper flanges. Regarding configuration J, 4 FE were used along the width (x-axis) of the lower flange and 2 FE in the upper flange. Configuration Ω was discretized with 2 FE along the width (x-axis) of each lower flange and with 3 FE on the upper flange.

Besides the additional stringers cross-sections, also two extra geometries of projectiles were considered: cylindrical and conical (Figure 3). The criterion for the design was that the diameter and mass were equal to those of the spherical projectile.

The cylindrical and conical projectiles were discretized with 1440 and 1776 FE, respectively.

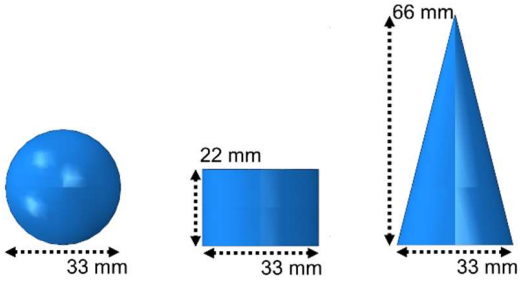

Figure 3: Geometry of different impactors: a) sphere, b) cylinder and c) cone.

3.2. Materials

The skin and stringers are made of CFRP IM7/8552 and the adhesive of Hexply 312.

Regarding the composite material, both elastic properties and strengths were those obtained by the COCOMAT project researchers [13], except for the density. The latter was obtained through the investigation carried out by Koerber and Camanho [14]. Regarding the fracture energy, the values proposed by Camanho *et al.* [15] were adopted. Table 1 shows the mechanical properties used to model the composite material. In Table 1: E_i - Young's modulus, ν_{ij} - Poisson's coefficient, G_{ij} - shear modulus, S_{ti} - tensile strength, S_{ci} - compressive strength, S_{sij} - shear strength, G_{ti} - tensile fracture energy, G_{ci} - compressive fracture energy and ρ - density. The mechanical properties are referred to local directions of the material (i,j = 1, 2 or 3).

Table 1: Mechanical properties of CFRP IM7/8552.

Elastic properties		Strengths	
E_1 [MPa]	147000	S_{t1} [MPa]	2715
E_2 [MPa]	11800	S_{c1} [MPa]	1400
ν_{12} [−]	0.34	S_{t2} [MPa]	56
G_{12} [MPa]	6000	S_{c2} [MPa]	25
G_{13} [MPa]	6000	S_{s12} [MPa]	101
G_{23} [MPa]	4000	S_{s23} [MPa]	131
ρ [kg/m³]	1590		
Fracture energies			
G_{t1} [N/mm]	81.5	G_{t2} [N/mm]	0.277
G_{c1} [N/mm]	106.3	G_{c2} [N/mm]	0.788

Regarding the damage and failure of the IM7/8552, the Hashin damage initiation criterion was used. It takes into account four possible failure modes with four corresponding indexes: (i) fibre breakage in tension (F_f^t), (ii) fibre kinking in compression (F_f^c), (iii) matrix cracking in tension (F_m^t) and (iv) matrix crushing in compression (F_m^c),

$$F_f^t = \left(\frac{\hat{\sigma}_{11}}{S_{t1}}\right)^2 + \alpha\left(\frac{\hat{\sigma}_{12}}{S_{s12}}\right)^2 \leq 1 \text{ and } \hat{\sigma}_{11} \geq 0 \quad (5)$$

$$F_f^c = \left(\frac{\hat{\sigma}_{11}}{S_{c1}}\right)^2 \leq 1 \text{ and } \hat{\sigma}_{11} < 0 \quad (6)$$

$$F_m^t = \left(\frac{\hat{\sigma}_{22}}{S_{t2}}\right)^2 + \left(\frac{\hat{\sigma}_{12}}{S_{s12}}\right)^2 \leq 1 \text{ and } \hat{\sigma}_{22} \geq 0 \quad (7)$$

$$F_m^c = \left(\frac{\hat{\sigma}_{22}}{2S_{s23}}\right)^2 + \left[\left(\frac{S_{c2}}{2S_{s23}}\right)^2 - 1\right]\frac{\hat{\sigma}_{22}}{S_{c2}} + \left(\frac{\hat{\sigma}_{12}}{S_{s12}}\right)^2 1 \text{ and } \hat{\sigma}_{22} < 0 \quad (8)$$

where $\hat{\sigma}_{11}$, $\hat{\sigma}_{22}$ and $\hat{\sigma}_{12}$ are the applied stresses, S_{ti}, S_{ci} and S_{sij} have the meaning previously explained and α is a coefficient $(0 \leq \alpha \leq 1)$ that accounts for the contribution of shear stress to the fibre breakage in tension. In this work, α = 1.0 is used.

Regarding the adhesive layer, the elastic properties adopted were also obtained during the COCOMAT project [16], except for the density. For the density was assumed a typical value for epoxy resins [2]. In Table 2 the mechanical properties used to model the adhesive can be observed: E, G, ν and ρ have the same meaning previously explained, t_n^0, t_s^0 e t_t^0 are the adhesive strengths and G_{IC}, G_{IIC} e G_{IIIC} represent the fracture energies for modes I, II and III, respectively.

Table 2: Mechanical properties of the adhesive - Redux 312.

Elastic properties		Strengths	
E [MPa]	3000	t_n^0 [MPa]	8.3
G [MPa]	1071	t_s^0 [MPa]	38.0
ν [−]	0.4	t_t^0 [MPa]	38.0
ρ [kg/m³]	1200		
Fracture energies			
G_{IC} [N/mm]	0.2		
G_{IIC} [N/mm]	1.0		
G_{IIIC} [N/mm]	1.0		

Regarding the damage initiation, the maximum nominal stress criterion was adopted, given by,

$$\max\left\{\frac{t_n}{t_n^0}, \frac{t_s}{t_s^0}, \frac{t_t}{t_t^0}\right\} = 1 \quad (9)$$

where t_n, t_s e t_t are applied stresses and t_n^0, t_s^0 and t_t^0 have the meaning previously explained. A mixed-mode damage evolution law based on the Benzeggagh-Kenane criterion, with a power coefficient of 4.5, was also adopted.

The elastic properties of steel and ice used to model the projectiles are shown in Table 3 [8,17].

Table 3: Elastic properties of steel [8] and ice [17].

	Steel	Ice
E [MPa]	210000	938
ν [−]	0.30	0.33
ρ [kg/m^3]	7850	900

3.3. Loading, boundary conditions and analysis procedure

All the panels studied are made by 3 parts, skin, adhesive and stringers, as mentioned. Hence, to ensure the skin/adhesive and stringers/adhesive connections, the TIE command was used.

The interaction between the projectile and the panel, resulting from the impact of the first in the second, was insured by Hard Contact instruction in the normal direction and by Friction in the tangential direction, with the adoption of a coefficient of friction of 0.3.

The boundary conditions used in this work are shown in Figure 1. The right edge was clamped whereas on the left edge all movements were restricted except for displacement along z-axis. In the first 60 mm of both ends, all displacements and rotations were restrained except for the longitudinal displacement (z-axis). For the projectile, an initial velocity was imposed along y-axis and all displacements except that in which velocity was imposed were restrained. All the boundary conditions described above were common to all analyses. The remaining (pressure and/or applied force) are dependent on the type of preload. If the intention is to study the influence of tension/compression loading on the panel's behaviour, the desired load level (P) is applied to the left edge (along z-axis).To study the effect of pressurization, in addition to the internal pressure (P_i), the hoop stress (σ_H) that arises is also considered. Thus, discounting the first 60 mm of both ends, the internal pressure (P_i) is applied along the skin and flanges and the hoop stress (σ_H) is applied on the skin's longitudinal edges.

3.4. Strain-rate dependent properties of carbon/epoxy composite

To implement the dependence of the composite's mechanical properties on strain rate, the model proposed by Schaefer *et al.* [11], described before, was used to affect all elastic properties and strengths. However, since Abaqus [12] does not allow the implementation directly of strain dependence using Hashin damage initiation criterion, the analysis was done in two parts.

Firstly, the panel was modelled with quasi-static properties and the Hashin criterion. Then, selecting only the elements that would be damaged due to the impact, the strain rates in directions 1 and 2 were obtained for each time increment. To guarantee the contribution of both directions, the strain rate was calculated as follows,

$$\mathrm{ER}(t) = \sqrt{\left(\mathrm{ER}_{11}(t)\right)^2 + \left(\mathrm{ER}_{22}(t)\right)^2} \qquad (10)$$

where $\mathrm{ER}_{11}(t)$ and $\mathrm{ER}_{22}(t)$ correspond to the strain rates in directions 1 and 2, respectively.

Additionally, the average value of $\mathrm{ER}(t)$ was computed, discarding the null values, up to the increment in which any given type of damage was initiated according to Hashin's criterion. Based on this average value, all elastic properties and strengths were recalculated according to that proposed by Schaefer *et al.* [11]. Finally, the finite element model was modified considering the strain rate dependent properties and a second simulation was made to obtain the residual velocity (V_R) of the projectile.

3.5. Validation of the models

Since this work had no experimental results to be compared with the numerical ones, one additional model was developed. Therefore, to validate the finite element model, the one developed by Pernas-Sánchez *et al.* [8] was replicated since it has similar modelling options to those adopted.

The replica developed had the same dimensions, materials and boundary conditions used experimentally by Pernas-Sánchez *et al.* [8]. However, for the fracture energies, the values proposed by Camanho *et al.* [15] were assumed, since Pernas-Sánchez *et al.* [8] did not consider intralaminar failure modes in their work. Regarding the finite element mesh, S4 shell FE and C3D8 hexahedral solid FE were adopted to discretize, respectively, the plate and the projectile.

Then, the influence of strain rates on the mechanical properties of the composite was investigated by three models: one considering the dependence (between mechanical properties and the strain rate) as proposed by Schaefer *et al.* [11],

a model without the relation of Schaefer *et al.* [11] and a model adapting the Schaefer *et al.* [11] relation to all elastic properties and strengths. As can be seen in Figure 4, it appears that all approaches lead to similar predictions of residual velocity of the projectile for a given impact velocity. For reduced velocities, the results obtained without the relation proposed by Schaefer *et al.* [11] are closer to the experimental values. However, this trend does not occur for higher velocities, in which the adaptation of the relationship (between properties and strain rate) presents a closer prediction to the experimental one. Hence, it was decided to use the adaptation of the relation in the remaining simulations.

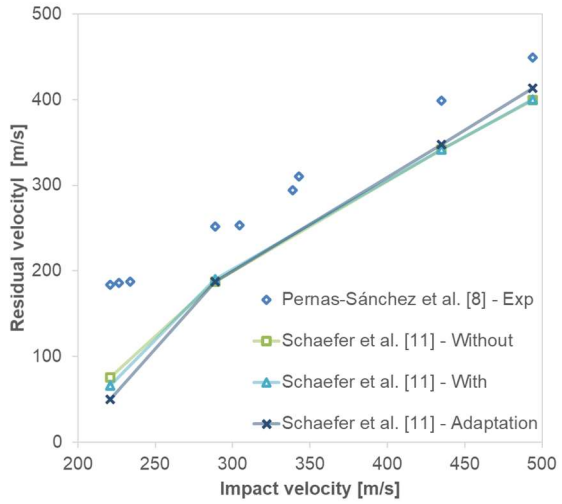

Figure 4: Replica's results and results by Pernas-Sánchez *et al.* [8] for several impact velocities.

4. Numerical results

4.1. Parametric studies on the reference panel impacted by steel projectiles

Figure 5 shows the influence of the projectile's geometry for 3 initial velocities: 75, 100 and 150 m/s. As it may be observed, for lower velocities the projectile that most easily penetrates the panel is the conical-shaped. However, for velocities above 100 m/s, the behaviour induced by spherical and conical projectiles is similar. Since both projectiles have the same kinetic energy, this difference seems to indicate that for lower velocities, the longer the time needed to reach the maximum impact area of the projectile, the higher the residual velocity. Also, the cylindrical projectile is the one that presents the most difficulty in the perforation of the panel. This behaviour suggests that the larger the impact area, at the time of the collision, the lower the residual velocity.

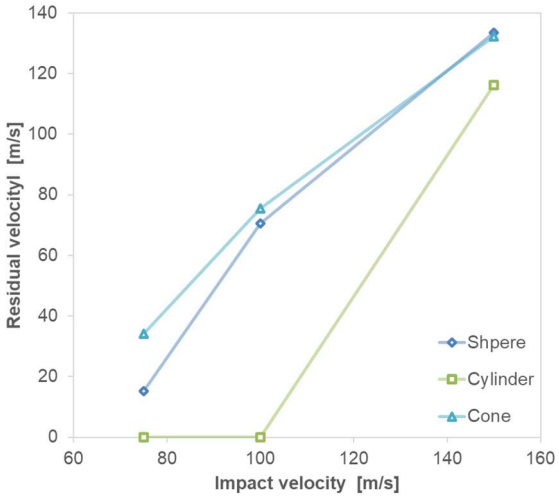

Figure 5: Influence of the steel projectile geometry on the reference panel.

For the conical geometry, a more detailed analysis of the results is presented, considering the damage and the influence of preloads. Regarding the damage, as seen in Figure 6 a), the mechanism that contributes to the impact resistance of the panel is the bending of the skin, adhesive and stringers. The failure mechanism was plotted for the first instant in which the velocity of the projectile became constant.

To account the influence of preloads (in compression), besides the unstressed panel, the impact was also considered with 15 and 30% of the buckling load. The buckling load (P_{cr}) was obtained using Abaqus [12] (P_{cr} = 46.01 kN). As seen in Figure 7, for lower impact velocities (75 m/s), the introduction of preloads leads to higher residual velocities, with the most severe load being 15% of the buckling load. For the remaining impact velocities, the residual velocities are similar. This behaviour appears to be justified by the failure mechanism. For reduced velocities, the bending of the panel increases. This behaviour induces greater stresses (in tension and compression) on both sides of the panel. Therefore, introducing compressive preloads can reduce the strength of the panel if it fails due to compression of the fibres. For higher impact velocities, even if the failure mechanism continues to be the bending of the panel, it does not seem to influence the resistance of the panel as much.

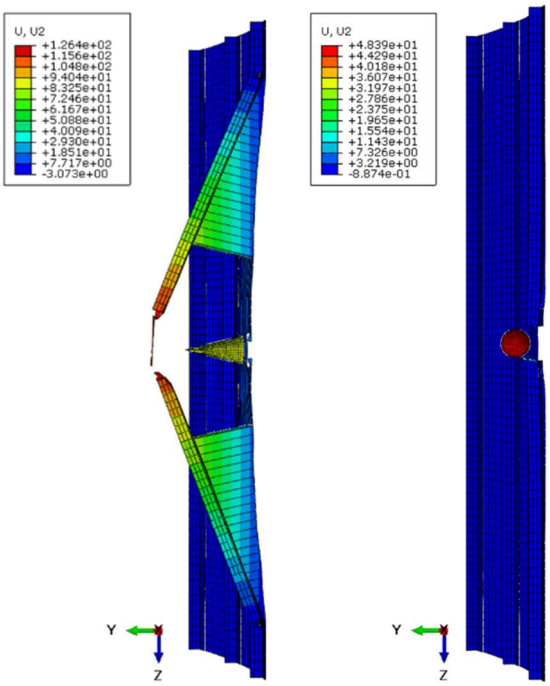

a) b)

Figure 6: Failure mode of reference panel for a) vi=75 m/s and b) vi=400 m/s.

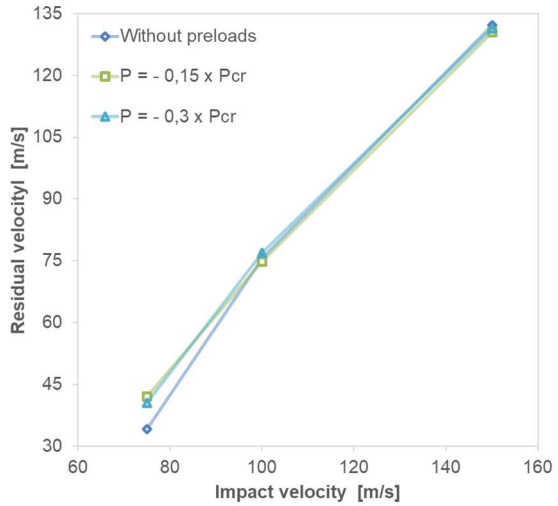

Figure 7: Influence of preloads in compression with steel projectiles.

Besides the preloads in compression, the same load values were also used in tension. Figure 8 shows that, like in compression, the residual velocity presents a higher dependence on the preloads for lower impact velocities, being nearly invariant for the remaining velocities. Also, the most demanding level is again 15% of the buckling load. The higher differences for lower velocities seem to be justified again by the failure mechanism. As previously mentioned, for lower impact velocities, the bending of the panel is significant, so, there is an increase in stresses on both sides of the panel. Therefore, introducing preloads in tension can reduce the resistance of the panel if it fails due to fibre tension.

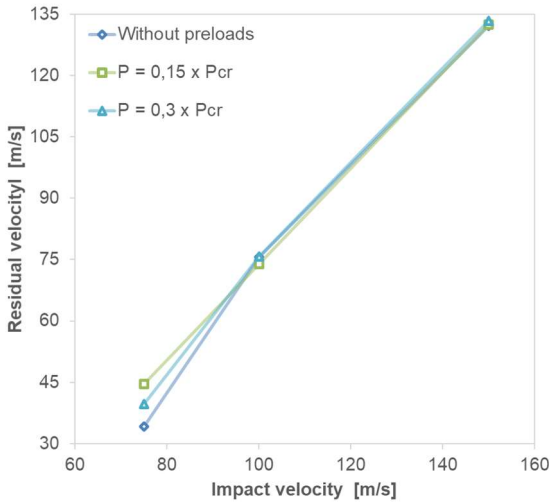

Figure 8: Influence of preloads in tension with steel projectiles.

4.2. Parametric studies on the reference panel impacted by ice projectiles

As for impacts with steel projectiles, the same 15 and 30% of the buckling load were considered in compression (Figure 9) and in tension (Figure 10) with an impactor made of ice. However, in this case, different impact velocities were used: 150, 250 and 400 m/s. As can be seen in both figures, for an impact velocity (V_i) of 150 m/s, in neither case the panel is perforated. For an impact velocity of 250 m/s, it appears that for preloads in compression, the residual velocity (V_R) is lower than that for the unstressed condition. However, for preloads in tension the residual velocities are found to be similar for the three loading levels. For V_i = 400 m/s, both preloaded conditions present residual velocities higher than the situation without preloads. Also, for both conditions (in compression and in tension) the load level with 30% of P_{cr} presents higher residual velocities.

To investigate the influence of pressurization, internal pressures of 25 and 50 kPa were considered. Besides the internal pressure, the effect of the hoop stress in the skin was also considered (see Figure 1). Figure 11 shows the influence of the pressurization on the residual velocity. For lower velocities, as in the other simulations with ice projectiles, in neither case the panel is perforated. For average velocities and in

both cases where the effect of pressurization was considered, the residual velocities are similar but lower than that for the unstressed case. For an impact velocity of 400 m/s, the residual velocity is higher for both pressurizations. Also, it appears that the condition with 50 kPa induces residual velocities slightly higher than the other conditions.

Unlike steel projectiles, where the failure mechanism was the bending of the skin, adhesive and stringer, for an unstressed panel impacted by ice, the damage is more localized in the vicinity of the impact area, as can be seen in Figure 6 b).The failure mechanism was plotted for the first instant in which the velocity of the projectile became constant.

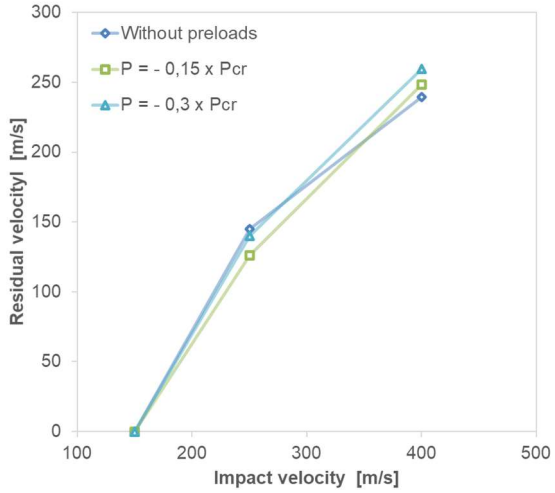

Figure 9: Influence of preloads in compression with ice projectiles.

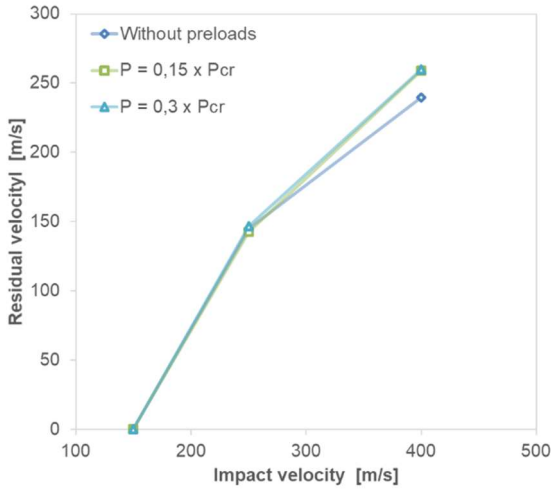

Figure 10: Influence of preloads in tension with ice projectiles.

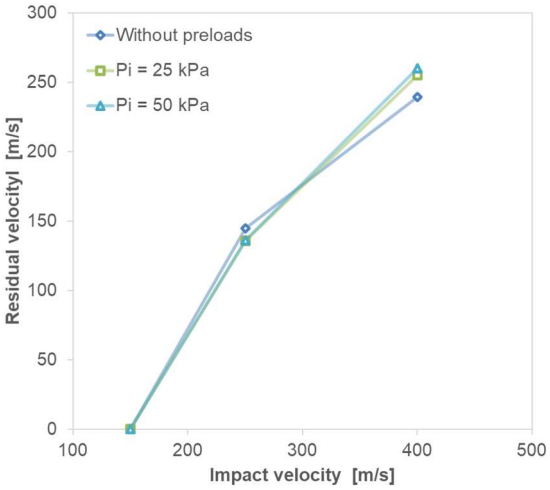

Figure 11: Influence of pressurization with ice projectiles.

4.3. Influence of stringer geometry

To investigate the influence of the stringer geometry, the most severe loading levels for the reference panel (with T-shaped stringers) were used in panels with I-, C-, J- and Ω-shaped stringers. Table 4 shows the buckling loads for the remaining panels, obtained using Abaqus [12].

Table 4: Buckling loads for the I-, C-, J- and Ω-shaped stringers.

Stringer	I	C	J	Ω
P_{cr} [kN]	38.79	38.57	41.52	56.49

Firstly, the same impact velocities adopted in the simulations with steel conical projectiles were consider, but now with a preload of 15% of P_{cr} in tension. As it may be observed in Figure 12, the panel with Ω-shaped stringers is the most resistant geometry and the C-shaped stringer is the one more easily perforated. As mentioned before, Fonseca *et al.* [9] concluded that the I-shaped stringer leads to the most resistant panel. However, as mentioned by the authors, the resistance was due to its greater cross-sectional area in comparison to the other geometries. In this work, since the same cross-sectional area and same height of the blades were used, the resistance of the panel must be influenced by the position and number of blades. The C-shaped stinger appears to be, on average, less resistance because the blade position is offset 8 mm from the impact point, which leads to a stringer rotation, not damaging the upper flange. Regarding Ω-shaped stringers, the resistance is due to its second blade that restrains the stringer rotation.

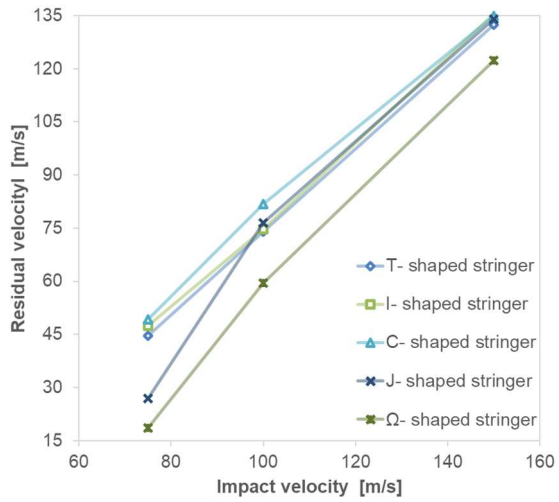

Figure 12: Influence of stringer geometry with steel projectiles.

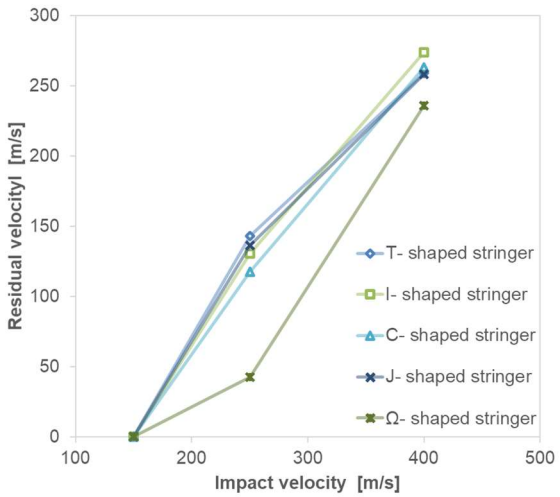

Figure 13: Influence of stringer geometry with ice projectiles.

For ice projectiles the conditions that were found to be more severe for the T-shaped stringer were also replicated for the remaining geometries. However, in this case, in addition to the preload with 30% of the buckling load applied in tension (more severe level), the more aggressive pressurization effect is also introduced (50 kPa). As can be seen in Figure 13, for V_i = 150 m/s, no panel is penetrated. For an impact velocity of 250 m/s, the panel with Ω-shaped stringers results in residual velocities considerably lower than those of the other panels. Also, the most easily perforated panel is the one with T-shaped stringers. For an impact velocity of 400 m/s, the panel with Ω-shaped stringers remains the most resistant panel and the panel with I-shaped stringers is the most easily perforated. Also, the behaviour of T-, I, C- and J-shaped stringers is similar for all the impact velocities considered. For ice projectiles, contrary to impacts with steel, the C-shaped stringers do not rotate. This result seems to indicate that the rotation of the stringer could be related to the projectile's geometry. Nevertheless, the Ω-shaped stringers are, on average, the most resistant. For high impact velocities the residual velocity obtained is close to those obtained for the other panels. This result seems to suggest that for higher velocities the stringer geometry is not as important as before, and only the amount of material of the stringers influences the resistance.

5. Conclusions

In this work, a numerical model was developed to study the mechanical behaviour of composite fuselage panels under impact loadings. Five panels (with T-, I-, C-, J and Ω-shaped stringers) were studied to determine which stringer makes the panel more resistant to impact. For all simulations, the effect of the strain rate on the panel was introduced and for both projects (steel and ice) only their elastic properties were considered.

For steel projectiles, the conical geometry induces, on average, higher residual velocities than the spherical and cylindrical ones. Additionally, for lower velocities, the longer the time needed to reach the maximum impact area of the projectile, the higher the residual velocity.

For conical steel projectiles, the introduction of 15% of the buckling load in tension leads, on average, to a lower resistance of the panel. For spherical ice projectiles, the level of 30% of the buckling load in tension is more severe. Also, for steel, the failure mechanism of the panel is the bending of skin, adhesive and stringers and for ice the damage is more localized.

The Ω-shaped stringer is found to be the most resistant geometry (both for steel and ice). Also, for steel projectiles, the C-shaped stringer rotates, however, the same does not occur for ice projectiles, which means that this rotation may be related to the projectile's geometry. Finally, for higher velocities with ice projectiles, the stringer geometry seems to be irrelevant and just the amount of material of the stringer seems to influence the residual velocity.

References

[1] A. P. Mouritz, *Introduction to Aerospace Materials*, 1st ed., Woodhead Publishing Limited, UK, 2012.

[2] S. R. Reid and G. Zhou, *Impact Behaviour of Fibre-Reinforced Composite Materials and Structures*, 1st ed., Woodhead Publishing Limited, England, 2000.

[3] H. Abramovich and C. Bisagni, "Behavior of curved laminated composite panels and shells under axial compression," *Progress in Aerospace Sciences,* vol. 78, pp. 74-106, 2015.

[4] P. M. Sforza, *Commercial Airplane Design Principles*, 1st ed., Elsevier, UK, 2014.

[5] A. H. Sheikh, P. H. Bull and J. A. Kepler, "Behaviour of multiple composite plates subjected to ballistic impact," *Composites Science and Technology,* vol. 69, nº 6, pp. 704-710, 2009.

[6] J. Pernas-Sánchez, J. A. Artero-Guerrero, D. Varas and J. López-Puente, "Experimental analysis of normal and oblique high velocity impacts on carbon/epoxy tape laminates," *Composites Part A: Applied Science and Manufacturing,* vol. 60, pp. 24-31, 2014.

[7] M. A. Silva, C. Cismaşiu and C. G. Chiorean, "Numerical simulation of ballistic impact on composite laminates," *International Journal of Impact Engineering,* vol. 31, nº 3, pp. 289-306, 2005.

[8] J. Pernas-Sánchez, J. A. Artero-Guerrero, J. Zahr Viñuela, D. Varas and J. López-Puente, "Numerical analysis of high velocity impacts on unidirectional laminates," *Composite Structures,* vol. 107, pp. 629-634, 2014.

[9] F. Fonseca, A. P. C. Duarte and N. Silvestre, "Finite element modeling of CFRP fuselage panels under high velocity transverse impact loading," in *Advances in Engineering Materials, Structures and Systems: Innovations, Mechanics and Applications: Proceedings of the 7th International Conference on Structural Engineering, Mechanics and Computation*, Cape Town, South Africa (A. Zingoni, Ed.) pp. 449-454, Taylor and Francis, London, UK, 2019.

[10] J. M. C. d. F. Justo, *Estudo do Comportamento ao Impacto de Alta Velocidade de Estruturas em Materiais Compósitos*, PhD thesis. Faculty of Engineering, University of Porto, 2005.

[11] J. D. Schaefer, B. T. Werner and I. M. Daniel, "Strain-Rate-Dependent Failure of a Toughened Matrix Composite," *Experimental Mechanics,* vol. 54, nº 6, pp. 1111-1120, 2014.

[12] Simulia, *Abaqus User's Manual and Abaqus Theory Manual*, version 6.14, Dassault Systémes, Providence, RI, 2014.

[13] A. Winzen Referent, "Simulation of Stringer Stiffened CFRP Panels in Consideration of Skin-Stringer Separation," Aachen University of Applied Sciences, 2006.

[14] H. Koerber and P. P. Camanho, "High strain rate characterisation of unidirectional carbon-epoxy IM7-8552 in longitudinal compression," *Composites Part A: Applied Science and Manufacturing,* vol. 42, nº 5, pp. 462-470, 2011.

[15] P. P. Camanho, P. Maimí and C. G. Dávila, "Prediction of size effects in notched laminates using continuum damage mechanics," *Composites Science and Technology,* vol. 67, pp. 2715-2727, 2007.

[16] R. Degenhardt, A. Kling, K. Rohwer, A. C. Orifici and R. S. Thomson, "Design and analysis of stiffened composite panels including post-buckling and collapse," *Computers and Structures,* vol. 86, nº 9, pp. 919-929, 2008.

[17] L. A. Coles, A. Roy and V. V. Silberschmidt, "Ice vs. steel: Ballistic impact of woven carbon/epoxy composites. Part II – Numerical modelling," *Engineering Fracture Mechanics,* vol. 225, p. 106297, 2020.